View metadata, citation and similar papers at core.ac.uk

brought to you by CORE

provided by VCU Scholars Compass

Virginia Commonwealth University
VCU Scholars Compass

Electrical and Computer Engineering Publications | Dept. of Electrical and Computer Engineering

2008

Current versus voltage characteristics of GaN/AlGaN/GaN double heterostructures with varying AlGaN thickness and composition under hydrostatic pressure

I. P. Steinke
University of Minnesota

P. P. Ruden
University of Minnesota

X. Ni
Virginia Commonwealth University

H. Morkoç
Virginia Commonwealth University, hmorkoc@vcu.edu

K. A. Son
California Institute of Technology

Follow this and additional works at: http://scholarscompass.vcu.edu/egre_pubs

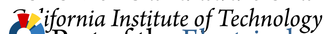

Part of the Electrical and Computer Engineering Commons

Steinke, I. P., Ruden, P. P., & Ni, X., et al. Current versus voltage characteristics of GaN/AlGaN/GaN double heterostructures with varying AlGaN thickness and composition under hydrostatic pressure. Journal of Applied Physics, 103, 064502 (2008). Copyright © 2008 American Institute of Physics.

Downloaded from

http://scholarscompass.vcu.edu/egre_pubs/146

This Article is brought to you for free and open access by the Dept. of Electrical and Computer Engineering at VCU Scholars Compass. It has been accepted for inclusion in Electrical and Computer Engineering Publications by an authorized administrator of VCU Scholars Compass. For more information, please contact libcompass@vcu.edu.

Current versus voltage characteristics of GaN/AlGaN/GaN double heterostructures with varying AlGaN thickness and composition under hydrostatic pressure

I. P. Steinke,[1,a)] P. P. Ruden,[1] X. Ni,[2] H. Morkoç,[2] and K.-A. Son[3]
[1]*Department of Electrical and Computer Engineering, University of Minnesota, Minneapolis, Minnesota 55455, USA*
[2]*Department of Electrical Engineering, Virginia Commonwealth University, Richmond, Virginia 23284, USA*
[3]*Jet Propulsion Laboratory, California Institute of Technology, Pasadena, California 91109, USA*

(Received 5 October 2007; accepted 12 December 2007; published online 17 March 2008)

We have studied current versus voltage characteristics of *n*-GaN/*u*-AlGaN/*n*-GaN double heterostructure devices under hydrostatic pressure up to 500 MPa. Devices were grown on *c*-plane sapphire substrates by organometallic vapor phase epitaxy using epitaxial layer overgrowth. The effect of AlGaN layer thickness and composition on the pressure sensitivity was investigated. For a fixed applied bias, we found that the current decreases approximately linearly in magnitude with increasing hydrostatic pressure over the range of voltages and pressures applied. The decrease in current magnitude can be attributed to piezoelectric effects and is consistent with model calculations. The polarization charge densities at the GaN/AlGaN interfaces change with hydrostatic pressure, which in turn modifies the internal potential barrier. Changes in the AlGaN layer thickness and composition also modify the interfacial polarization, with thicker AlGaN layers and higher AlN content increasing the effect of pressure on the observed current versus voltage characteristics. The strain gauge factors obtained for these devices range from ~200 to 800. © *2008 American Institute of Physics*. [DOI: 10.1063/1.2844484]

I. INTRODUCTION

Group III-nitride semiconductors have demonstrated excellent performance in high power and high frequency devices, optical emitters, and detectors.[1–3] The properties of these semiconductor materials are ideal for use at high temperatures and in harsh environments. In particular, the large piezoresistive and piezoelectric constants of III-nitrides are attractive properties for stress sensing purposes. These particular properties have been explored in the study of piezoresistivity in *p*-GaN,[4] the change of Schottky barrier heights on *n*-GaN,[5] and *n*-AlGaN (Ref. 6) with hydrostatic pressure and the effect of stress on the current-voltage characteristics of GaN/AlGaN-based heterostructure field effect transistors (HFETs).[7–9]

One of the contributions to polarization in III-nitrides is due to their wurtzite crystal structure, which allows for spontaneous polarization parallel to the hexagonal axis. Epitaxial films of GaN and AlGaN layers contribute an additional piezoelectric polarization arising from the lattice mismatches between the substrate and different III-nitride layers. These polarizations manifest themselves in a double heterostructure of GaN/AlGaN/GaN, which has polarization-induced charge densities at the two GaN/AlGaN interfaces with equal magnitudes but opposite sign. The polarization at the interface creates accumulation and depletion layers on either side of the AlGaN layer if the GaN layers are doped. Hence, the resulting energy band profile is asymmetric, even though the structure is compositionally symmetric.[10]

The induced accumulation layers have been utilized in GaN/AlGaN field effect transistors.[8,9,11] The large values of polarization sheet charge densities[11] of up to 2×10^{13} e/cm^2 make it possible to achieve a high-density two-dimensional electron gas (2DEG) close to the GaN/AlGaN interface. The electron transport is parallel to the GaN/AlGaN interface in these devices. Under an applied stress, the amount of polarization charge at the accumulated interface is changed, modifying the density of charge carriers in the 2DEG and thus modulating the conductance of the device.

Electron transport perpendicular to the GaN/AlGaN interface has not received as much attention.[12] The primary difficulty has been that high quality, low defect density materials are required to study the fundamental current mechanisms. Defects in the AlGaN barrier layer provide current leakage paths that can easily become the dominant transport mechanism. Nevertheless, GaN/AlGaN/GaN double heterostructure devices have been shown to be promising candidates for stress sensing applications.[10] The mechanisms for transport in the perpendicular direction are primarily limited by the effective barrier height for electron injection over the AlGaN barrier layer and the effective barrier width for tunneling through the barrier. An applied stress changes both the effective barrier height as well as the effective barrier width, which in turn modulates the magnitude of the current.

To explore these structures systematically, we have grown high quality GaN/AlGaN/GaN devices with varying AlN content and AlGaN barrier thickness. We have tested the stress sensing ability of these devices under hydrostatic pressure. In order to describe quantitatively the performance of

[a)]Author to whom correspondence should be addressed. Electronic Mail: stei0194@umn.edu.

[This article is copyrighted as indicated in the article. Reuse of AIP content is subject to the terms at: http://scitation.aip.org/termsconditions. Downloaded to] IP: 128.172.48.59 On: Wed, 04 Nov 2015 18:53:52

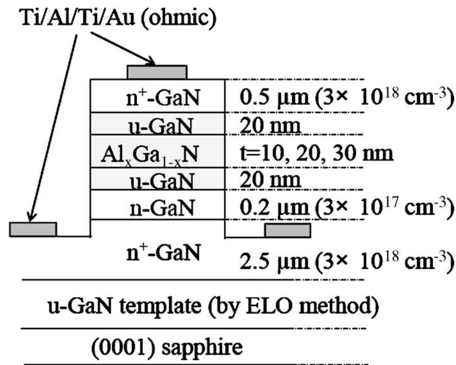

FIG. 1. GaN/AlGaN/GaN device structure.

the devices as pressure sensors, we define a suitable gauge factor. Results show comparable performance to III-nitride HFET-based stress sensors. We compare our results to a device model and explain the data with the aid of self-consistently calculated conduction band profiles.

II. EXPERIMENTAL RESULTS

Samples were grown on *c*-plane sapphire substrates by organometallic vapor phase epitaxy using epitaxial lateral overgrowth (ELO). A 2.5 μm thick n^+-GaN layer was grown on top of the ELO GaN template followed by multiple layers that make up the n-GaN/u-$Al_xGa_{1-x}N$/n-GaN double heterostructure shown in Fig. 1. In this work, we present results from samples with varying AlGaN barrier thicknesses and composition, as summarized in Table I. Devices were patterned into circular mesa structures of 200 μm in diameter and 1.2 μm in height using reactive ion etching. Further details of the growth and fabrication procedures may be found in Ref. 12.

For measurement of the current-voltage (*I*-*V*) characteristics under hydrostatic pressure, devices were wire bonded and mounted into a Unipress LC10 liquid cell provided by the Polish Academy of Sciences. The pressure transmitting medium was a 1:1 mixture of hexane and pentane. Pressure was applied to the devices with the aid of a Unipress LCP20 hydraulic press up to 500 MPa in roughly 100 MPa increments. The pressure was monitored via the change in resistance of an InSb semiconductor pressure gauge, and *I*-*V* characteristics were taken using an HP 4145B semiconductor parameter analyzer. Consistent with previously reported

TABLE I. $Al_xGa_{1-x}N$ layer composition and thickness, maximum pressure gauge factor (PGF), and maximum strain gauge factor (SGF) for the samples tested under hydrostatic pressure.

Sample parameters		Maximum	Maximum
x	t_{AlGaN} (nm)	PGF (GPa^{-1})	SGF
0.12	20	−0.628	494
0.15	10	−0.664	522
0.15	20	−0.594	467
0.15	30	−0.365	287
0.30	20	−1.06	832

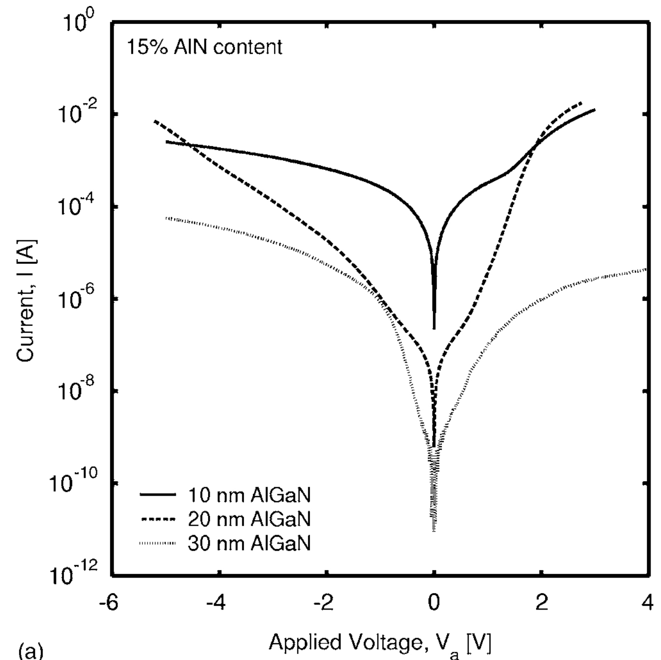

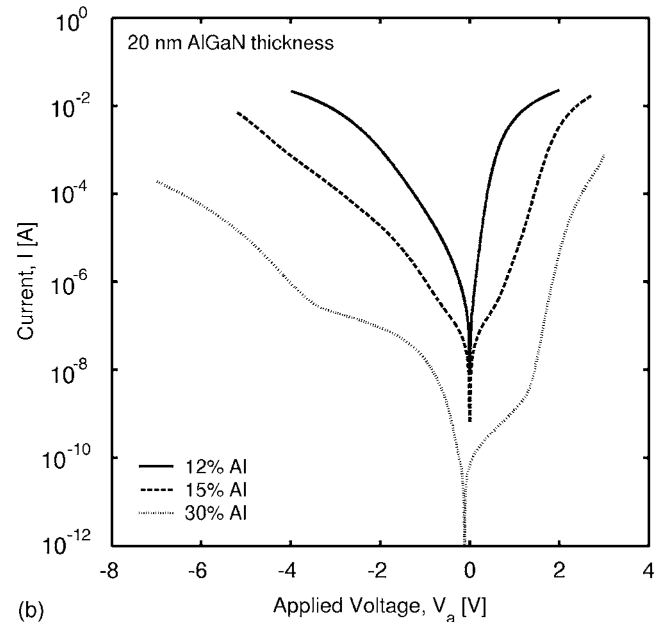

FIG. 2. (a) *I*-*V* characteristics at atmospheric pressure for devices with 15% AlN content and AlGaN layer thicknesses of 10, 20, and 30 nm. (b) *I*-*V* characteristics at atmospheric pressure with 20 nm AlGaN layer thickness and AlN contents of 12%, 15%, and 30%.

data,[10] all *I*-*V* characteristics were obtained with the top (mesa) contact grounded and the bias applied to the bottom (substrate) contact.

Figure 2(a) shows the atmospheric pressure *I*-*V* characteristics obtained from the samples with 15% AlN content and varying AlGaN thickness. For each of the three samples, we observed rectifying behavior attributable to the asymmetric internal potential barrier. Moreover, we observe that samples with small AlGaN barrier thickness have larger current magnitudes at most applied voltages, as expected. [The larger current magnitude observed in the 20 nm AlGaN sample over the 10 nm AlGaN sample in Fig. 2(a) at large

[This article is copyrighted as indicated in the article. Reuse of AIP content is subject to the terms at: http://scitation.aip.org/termsconditions. Downloaded to] IP: 128.172.48.59 On: Wed, 04 Nov 2015 18:53:52

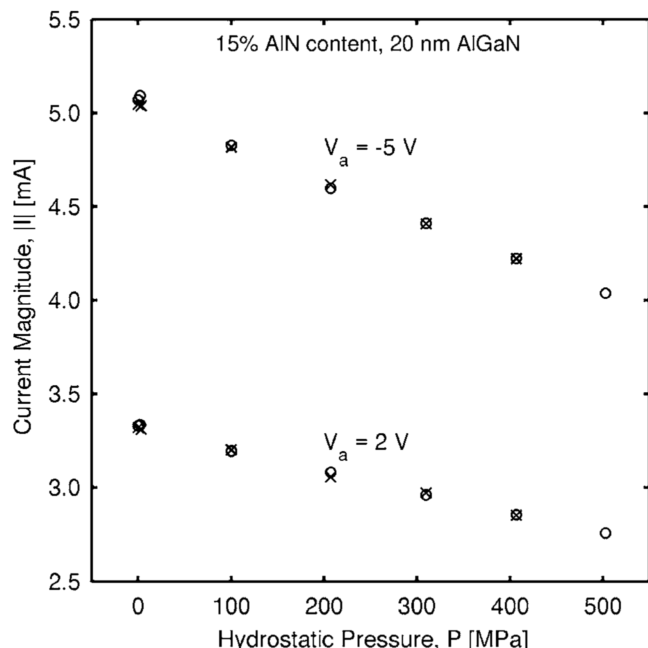

FIG. 3. Dependence of current magnitude on pressure for applied voltages of 2 and −5 V for the 15% AlN, 20 nm thick AlGaN layer device. Circles indicate data points taken after an increase in pressure of 100 MPa, while crosses indicate data points taken after a decrease in pressure of 100 MPa.

forward (>2 V) and reverse biases (<−4 V) is attributed to differences in series and contact resistances for the two samples.] Similarly, the *I-V* characteristics of the three samples with varying AlGaN composition and 20 nm AlGaN layer thickness at atmospheric pressure are plotted in Fig. 2(b). Again, we observed rectifying behavior for all three samples and larger current magnitude under all applied biases for structures with lower AlN content in the barrier layer.

The effects of hydrostatic pressure on the *I-V* characteristics obtained for these double heterostructures are illustrated in Fig. 3 for the sample with 15% AlN content and an AlGaN layer thickness of 20 nm. The sample shows a decrease in current magnitude that is linear over the range of pressures tested. Here, we have arbitrarily chosen two values of applied bias, +2 V and −5 V, to illustrate this decrease. The decrease in current magnitude is also observed for other values of applied bias. In Fig. 3, points plotted with open circles indicate that the data were taken after an increase in hydrostatic pressure of ~100 MPa, while points plotted with a cross indicate the data taken after a decrease in pressure of ~100 MPa. The relatively low scatter in these data points indicates that the pressure cycle is retraceable and that no potentially deleterious effects that lead to persistent changes in the sample took place during the entire pressure run. We obtained similar results with all other samples.

Typically, a "gauge factor" is used to characterize the performance of devices employed as stress sensors or strain gauges. In order to discuss the sensitivity of our devices, we define a pressure gauge factor (PGF) as a normalized current change per unit pressure,

$$\mathrm{PGF} = \frac{I(P) - I(0)}{I(0)} \cdot \frac{1}{P}, \tag{1}$$

where $I(0)$ is the current taken at atmospheric pressure and $I(P)$ is the current at hydrostatic pressure P. The PGF indicates the relative normalized change in current per unit pressure. However, it is also useful to evaluate the performance on a strain based metric rather than pressure based. Since the elastic response of these devices is dominated by the thick substrate,[10] we can convert the PGF to a strain gauge factor (SGF) by dividing the PGF by the pressure induced in-plane elastic strain of the substrate per unit applied pressure ($\varepsilon_{\parallel}/P$). Using the elastic constants for sapphire,[13] we calculate a pressure induced in-plane strain of -1.273×10^{-3} GPa^{-1}. In Fig. 3, the slope of each sequence of data points is proportional to the PGF at the respective applied voltages. A maximum PGF of -0.594 GPa^{-1} is obtained from the data for the 20 nm thick $Al_{0.15}Ga_{0.85}N$ sample; this converts to a maximum SGF of 467 for that sample. Table I lists the maximum pressure and SGFs obtained for each sample.

III. THEORETICAL MODEL AND DISCUSSION

We modeled the *I-V* characteristics for samples presented in this work. Solution of the model involves solving the Poisson equation self-consistently with appropriate boundary conditions at the AlGaN barrier interfaces.[14] Electron transport across the AlGaN barrier is assumed to be due to thermionic emission and tunneling processes, and regions outside the barrier are in local thermal equilibrium. The tunneling probability is calculated using a one-dimensional Wentzel–Kramers–Brillouin approximation. Donor levels in the *n*-type GaN layers are taken to be 30 meV below the conduction band edge. Further details of the model and procedure can be found elsewhere.[10]

The key parameters of the model include the AlGaN layer thickness and composition as well as the polarization charge densities at the AlGaN/GaN interfaces. To calculate the polarization charge densities, we have followed the procedure outlined by Ambacher *et al.*[15] We have assumed that all nitride layers are pseudomorphic to each other and that the initial n^+-GaN layer is strain-free. Under hydrostatic pressure, the thick substrate dominates the elastic response. The material constants presented in Ref. 15 have been used consistently in our calculations.

Figure 4 presents current density versus voltage (*J-V*) characteristics obtained from the model for the samples tested in this work. Again, results are shown for $Al_{0.15}Ga_{0.85}N$ with varying AlGaN thickness [Fig. 4(a)] and varying AlGaN composition with 20 nm AlGaN thickness [Fig. 4(b)]. We find that the current density increases with both decreasing AlGaN layer thickness and decreasing AlN content, similar to our experimental results. However, there are quantitative discrepancies between the model results and the experimental data. In particular, we note the large difference in current density between the $Al_{0.15}Ga_{0.85}N$ and $Al_{0.3}Ga_{0.7}N$ samples seen in the model calculations in Fig. 4(b) that is less prominent in the experimental results shown in Fig. 2(b). We attribute these differences to additional current paths that may exist in the samples, such as defect-

[This article is copyrighted as indicated in the article. Reuse of AIP content is subject to the terms at: http://scitation.aip.org/termsconditions. Downloaded to] IP: 128.172.48.59 On: Wed, 04 Nov 2015 18:53:52

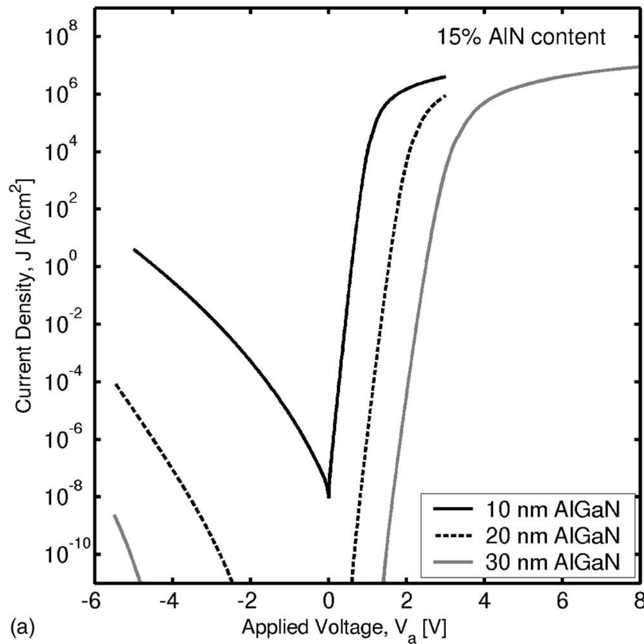

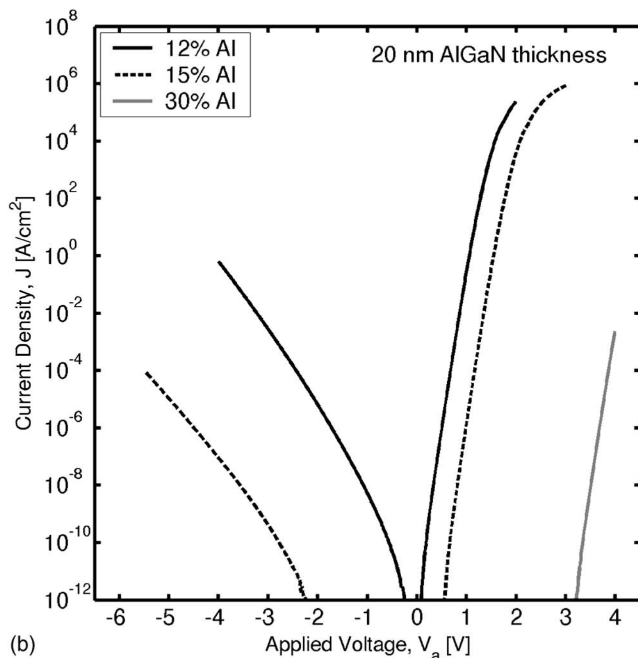

FIG. 4. (a) Calculated *J-V* curves for devices with 15% AlN content and varying AlGaN layer thickness, and (b) calculated *J-V* curves with 20 nm AlGaN thickness and varying AlN content.

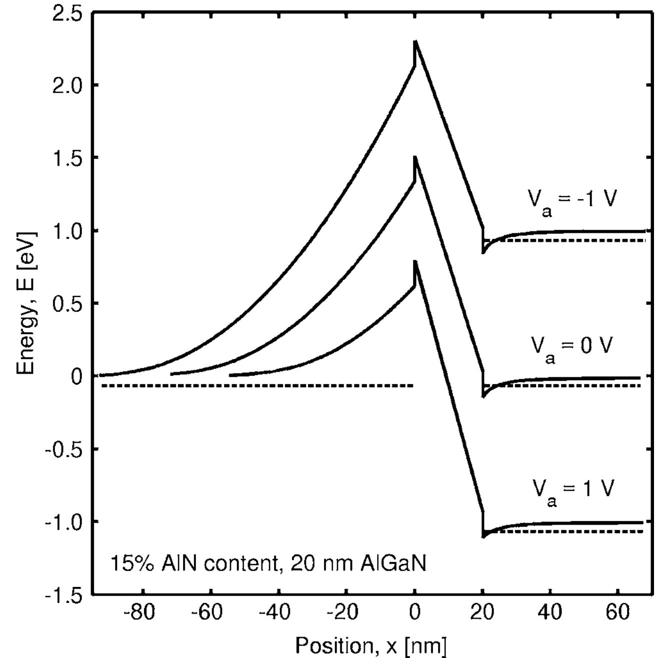

FIG. 5. Calculated band profiles for a 15% AlN, 20 nm thick AlGaN layer device under applied biases of −1, 0, and 1 V. Solid lines represent conduction band edges E_C and dashed lines indicate quasi-Fermi energies E_F in the top and bottom GaN layers.

assisted tunneling through the AlGaN layer or surface leakage on the etched vertical mesa, plausibly caused by the reactive ion etching process step. In addition, our calculation for the polarizations used an uncoupled electromechanical (EM) formulation rather than a coupled treatment.[16] Recent calculations[17] show that the coupled EM formulation reduces the piezoelectric polarization by up to 6.0% in $Al_{0.30}Ga_{0.70}N$. A reduction in the piezoelectric polarization would result in an increase in the current density and a better fit with experimental data.

In addition to *J-V* characteristics, we have also plotted the calculated conduction band profiles. The behavior of these devices is different in both the forward and reverse directions. In Fig. 5, the conduction band profiles for a 20 nm thick $Al_{0.15}Ga_{0.85}N$ device are presented. Under low forward bias ($<\sim 1$ V), the current consists of a combination of thermionic emission and tunneling. As a larger forward bias is applied to the device, the effective barrier width and the effective barrier height both decrease in magnitude, consequently increasing the contribution from both thermionic emission and tunneling mechanisms. However, the decrease in effective barrier width causes the current density to become primarily dominated by the tunneling mechanism. Under reverse bias, both mechanisms are again present at low applied voltages. However, as a larger reverse bias is applied, the thermionic emission component starts to become comparable and eventually exceeds the tunneling component as the effective barrier width increases.

The effects of AlGaN thickness on the conduction band profiles are presented in Fig. 6(a) for structures with 15% AlN content in the barrier. The conduction band profiles in Fig. 6(a) indicate that increasing the thickness primarily increases the effective barrier width. In addition, the effective barrier height also increases with increasing AlGaN layer thickness. This is a consequence of the voltage drop associated with the interface polarization charges that are only partially neutralized by the electron accumulation and depletion layers. The thicker AlGaN layers suppress the tunneling current component, requiring a larger bias to reach a given current level, consistent with Fig. 2(a).

Similarly, we observe that as the AlN content increased in the AlGaN layer, the voltage required to reach a given current also increases [Fig. 2(b)]. The increase in AlN content decreases the equilibrium lattice constant for the AlGaN layer, causing the in-plane tensile strain in the AlGaN layer to increase. The increase in the in-plane strain correspond-

[This article is copyrighted as indicated in the article. Reuse of AIP content is subject to the terms at: http://scitation.aip.org/termsconditions. Downloaded to] IP: 128.172.48.59 On: Wed, 04 Nov 2015 18:53:52

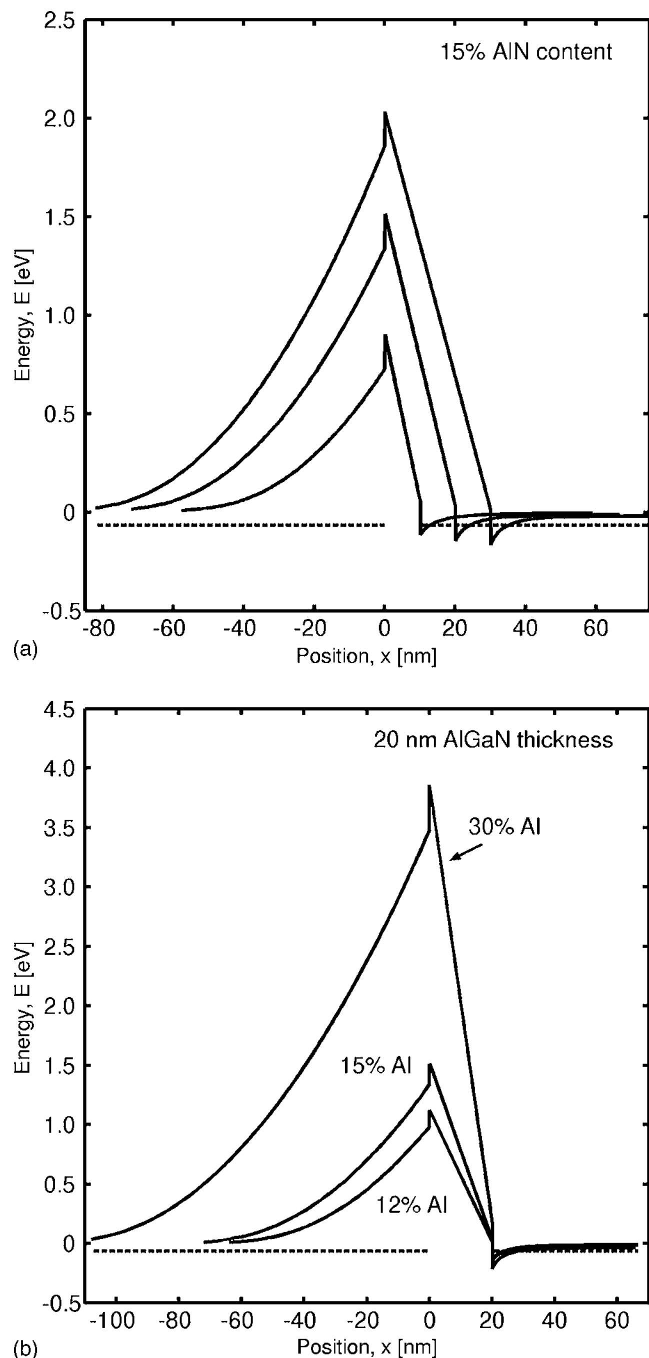

FIG. 6. Calculated equilibrium conduction band profiles (solid lines) for device with (a) 15% AlN content with varying AlGaN thickness and (b) 20 nm AlGaN layer thickness with varying AlN content. Dashed lines indicate Fermi energies E_F in the top and bottom GaN layers.

ingly increases the amount of polarization charge at both GaN/AlGaN interfaces along with the effective barrier height, which can be seen in Fig. 6(b). Since the thermionic emission mechanism is suppressed by the large energy barrier and the tunneling mechanism is suppressed by the wider effective barrier that includes the depletion layer, we expect a rather small current at low voltages. Clearly, "parasitic" current paths associated with the surfaces and with defects in the barrier become more important as the "intrinsic" current mechanisms considered in the model are weakened.

The total strain response of the sample under hydrostatic pressure includes an in-plane component ($\varepsilon_1=\varepsilon_2=\varepsilon_{\|}$) and an out-of-plane component (ε_3) that both increase in magnitude and are compressive. Due to the relative stiffness of the substrate, the net effect of these strain components is an increase in the polarization charge density at the GaN/AlGaN interfaces. This, in turn, increases the amount of band bending as well as the effective barrier height and effective barrier width, similar to the effect of increasing the AlN content [Fig. 6(b)]. Hence, for a fixed applied bias, the current should decrease as the hydrostatic pressure increases, as seen in Fig. 3.

The gauge factors we have presented in Table I compare favorably to our previously published results.[10] There, we observed SGFs in the range of 240–500 for a sample with a 10 nm $Al_{0.2}Ga_{0.8}N$ barrier. We would expect the pressure sensitivity of this sample to be slightly better than that of the sample with a 10 nm thick $Al_{0.15}Ga_{0.85}N$ barrier we tested in this work. However, the sample tested earlier had thicker undoped GaN spacer layers, which makes the direct comparison questionable. Indeed, the pressure responses of the two samples were quite similar.

IV. CONCLUSION

We have tested the pressure sensitivity of GaN/AlGaN/GaN double heterostructure devices under hydrostatic pressures up to 500 MPa. We found rectifying behavior for the *I*-*V* characteristics of all samples. Increasing the thickness of the AlGaN barrier layer or increasing the AlN content in the barrier layer lowers the current for a fixed applied bias. The reasons for this decrease are different for AlGaN thickness and composition. Thicker AlGaN layers require a larger bias before the effective barrier width becomes small enough for significant tunneling to occur. Whereas for AlGaN layers with larger AlN content, the increase in the lattice mismatch increases the strain and the piezoelectric charge at both AlGaN/GaN interfaces, leading to an increase in both the effective barrier height and effective barrier width. Similarly, application of hydrostatic pressure to these devices also increases the magnitudes of the piezoelectric polarization charge densities at the interfaces, causing the current to decrease as the pressure is increased. We calculated SGFs to characterize the performance of these samples and obtained values in the range of ~200–800. This compares favorably with samples previously tested and with other published results for III-nitride strain sensors.

ACKNOWLEDGMENTS

Partial support from NASA/PIDDP is gratefully acknowledged.

[1]H. Morkoç, *Handbook of Nitride Semiconductors and Devices* (Wiley-VCH, Berlin, 2008).
[2]*Wide Energy Bandgap Electronic Devices*, edited by F. Ren and J. C. Zolper (World Scientific, Singapore, 2003).
[3]O. Ambacher, J. Phys. D **31**, 2653 (1998).
[4]Y. Liu, M. Z. Kauser, M. I. Nathan, P. P. Ruden, A. M. Dabiran, B. Hertog, and P. P. Chow, Appl. Phys. Lett. **81**, 3398 (2002).
[5]Y. Liu, M. Z. Kauser, M. I. Nathan, P. P. Ruden, S. Dogan, H. Morkoç, S. S. Park, and K. Y. Lee, Appl. Phys. Lett. **84**, 2112 (2004).
[6]Y. Liu, M. Z. Kauser, P. P. Ruden, Z. Hassan, Y. C. Lee, S. S. Ng, and F.

[This article is copyrighted as indicated in the article. Reuse of AIP content is subject to the terms at: http://scitation.aip.org/termsconditions. Downloaded to] IP: 128.172.48.59 On: Wed, 04 Nov 2015 18:53:52

K. Yam, Appl. Phys. Lett. **88**, 022109 (2006).
[7]Y. Liu, P. P. Ruden, J. Xie, H. Morkoç, and K.-A. Son, Appl. Phys. Lett. **88**, 013505 (2006).
[8]B. S. Kang, S. Kim, F. Ren, J. W. Johnson, R. J. Therrien, P. Rajagopal, J. C. Roberts, E. L. Piner, K. J. Linthicum, S. N. G. Chu, K. Baik, B. P. Gila, C. R. Abernathy, and S. J. Pearton, Appl. Phys. Lett. **85**, 2962 (2004).
[9]S. N. G. Chu, F. Ren, S. J. Pearton, B. S. Kang, S. Kim, B. P. Gila, C. R. Abernathy, J.-I. Chyi, W. J. Johnson, and J. Lin, Mater. Sci. Eng., A **409**, 340 (2005).
[10]Y. Liu, M. Z. Kauser, D. D. Schroepfer, P. P. Ruden, J. Xie, Y. T. Moon, N. Onojima, H. Morkoç, K.-A. Son, and M. I. Nathan, J. Appl. Phys. **99**, 113706 (2006).
[11]O. Ambacher, B. Foutz, J. Smart, J. R. Shealy, N. G. Weimann, K. Chu, M. Murphy, A. J. Sierkowski, W. J. Schaff, L. F. Eastman, R. Dimitrov, A. Mitchell, and M. Stutzmann, J. Appl. Phys. **87**, 334 (2000).
[12]X. Ni, J. Xie, Y. Fu, H. Morkoç, I. P. Steinke, Y. Liu, P. P. Ruden, K.-A. Son, and B. Yang, Proc. SPIE **6473**, 11 2007.
[13]R. E. Hankey and D. E. Schuele, J. Acoust. Soc. Am. **48**, 190 (1970).
[14]K. Yang, J. R. East, and G. I. Haddad, Solid-State Electron. **36**, 321 (1993).
[15]O. Ambacher, M. Eickhoff, A. Link, M. Hermann, M. Stutzmann, F. Bernardini, V. Fiorentini, Y. Smorchkova, J. Speck, U. Mishra, W. Schaff, V. Tilak, and L. F. Eastman, Phys. Status Solidi C **0**, 1878 (2003).
[16]B. Jogai, J. D. Albrecht, and E. Pan, J. Appl. Phys. **94**, 6566 (2003).
[17]A. F. M. Anwar, R. T. Webster, and K. V. Smith, Appl. Phys. Lett. **88**, 203510 (2006).

[This article is copyrighted as indicated in the article. Reuse of AIP content is subject to the terms at: http://scitation.aip.org/termsconditions. Downloaded to] IP: 128.172.48.59 On: Wed, 04 Nov 2015 18:53:52